

SRF GUN CHARACTERIZATION - PHASE SPACE AND DARK CURRENT MEASUREMENTS AT ELBE*

E. Panofski[#], A. Jankowiak, T. Kamps, Helmholtz-Zentrum Berlin, Berlin, Germany
P.N. Lu, J. Teichert, Helmholtz-Zentrum Dresden-Rossendorf, Dresden, Germany

Abstract

RF photoelectron sources with superconducting cavities provide the potential to generate high quality, high brightness electron beams for future accelerator applications. At Helmholtz-Zentrum Dresden-Rossendorf, such an electron source was operated for many years. The commissioning of an improved SRF Gun with a new high-performance gun cavity with low field emission and a superconducting solenoid inside the gun cryomodule (SRF Gun II) has started in June 2014. First low current measurements as well as studies of unwanted beam transport using SRF Gun II with a Cu photocathode and an acceleration gradient up to 7 MV/m will be presented. First longitudinal beam characterization of the SRF Gun in combination with ELBE, a two-stage superconducting linear accelerator will be discussed.

INTRODUCTION

Helmholtz-Zentrum Dresden-Rossendorf has provided a test stand for SRF gun technology since 2007. Furthermore, this SRF gun can also be used as an electron source for the two-stage superconducting linear accelerator ELBE. In order to reach a higher acceleration field in the cavity and therefore peak electron energy, a new high-performance gun cavity attended by a superconducting solenoid was assembled in the gun cryomodule in May 2014 [1]. For successful application of the new injector commissioning and full beam characterization of SRF Gun II is required. The presented low current measurements focus on longitudinal phase space characterization and first studies about unwanted beam transport.

For future applications, such as driving X-Ray FEL facilities, the longitudinal phase space distribution plays a critical role. Therefore, good understanding of the longitudinal phase space of the photoelectron source is required. The new high-performance gun cavity design of the photoinjector offers low field emission which will be investigated by measuring dark current from SRF Gun II. Unwanted beam transport to the ELBE beamline is determined by the energy acceptance of the dogleg.

This paper starts with a short overview about the design parameters of the SRF gun as well as the relevant operation parameters of the photoinjector in combination with the linear accelerator ELBE. A review of the experimental technique measuring the longitudinal phase space, followed by a description of the data analysis method is given. All experimental results for the longitudinal phase space are presented. The final section

* Work supported by BMBF & Land Berlin

[#] eva.panofski@helmholtz-berlin.de

of this paper will summarize first studies of the energy acceptance of the dogleg and therefore the transport of dark current, generated by the SRF gun, into the ELBE beamline.

COMMISSIONING OF THE SRF GUN

All beam characterization measurements are done with the SRF Gun II in combination with two-stage linear accelerator ELBE. Figure 1 represents the schematic setup.

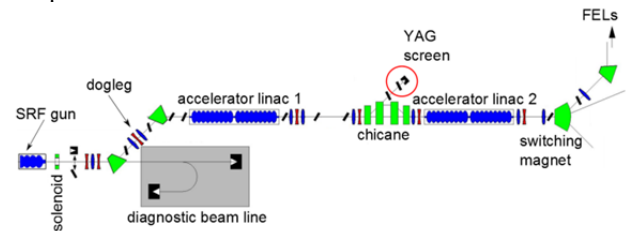


Figure 1: SRF Gun and ELBE beamline at HZDR Dresden [2].

Setup and Operation Parameters

The 1.3 GHz Nb gun cavity consists of 3.5 TESLA cells with a normal conducting Cu photocathode installed in the backplane of the half cell. In order to suppress multipacting a DC bias voltage is applied on the photocathode. The cathode is illuminated by 266 nm UV laser light. The drive laser provides 6 ps (rms) long laser pulses with a repetition rate of 100 kHz and an approximately uniform, 2mm transverse profile [1]. Due to the low quantum efficiency of the copper cathode ($\sim 10^{-5}$) only low bunch charges typically smaller than 5 pC are achieved. Therefore, space charge effects can be neglected for all measurements presented in this paper. The generated electron beam is accelerated with maximum gradient (peak field) of 18 MV/m corresponding to a kinetic energy of 3.5 MeV at the gun exit.

Afterwards, the electron beam is guided through the achromatic dogleg to ELBE beamline. The dogleg consists of two bend magnets attended by three quadrupoles which control the horizontal dispersion. The final acceleration up to 19 MeV takes place in the two superconducting cavity modules (C1, C2) of ELBE Linac 1. For all longitudinal phase space measurements presented in this paper the first dipole of the chicane is used to deflect the electron beam with a bend angle of 45° to the YAG screen in the diagnostic beamline.

All relevant measurement conditions and machine settings are summarized in Table 1.

Table 1: Parameters of SRF Gun II and ELBE

SRF Gun		
Laser wavelength	λ	266 nm
Laser rep. rate	f_{Laser}	100 kHz
Laser pulse length	σ_{Laser}	6 ps
DC bias cathode	V_{bias}	-5 kV
Field (peak)	E_{acc}	7 MV/m (18 MV/m)
ELBE		
Gradient C1	$E_{\text{acc}}(\text{C1})$	9.7 MV/m
Gradient C2	$E_{\text{acc}}(\text{C2})$	5.3 MV/m

Commissioning of SRF Gun II

The longitudinal phase space of the SRF Gun II can be evaluated at the diagnostic beamline of the photoinjector [3]. Using the 180° dipole together with a YAG screen the energy as well as the energy spread at the gun exit can be determined as function of laser phase. This measurement was done for two different laser phases, 49.4° and 56.6°. The kinetic energy for both phases is 3.59 MeV. After calibrating the screen, an energy spread of $23.04 \pm 0.96 \text{ keV}$ is found for 49.4° laser phase while 56.6° corresponds to an energy spread of $13.44 \pm 0.96 \text{ keV}$.

The emission length can be estimated by measuring the beam current with a Faraday Cup while varying the laser phase. This so called Schottky Scan for a maximum laser intensity (fully open aperture) and two different DC bias voltages 0 kV and -5 kV is shown in Fig. 2. The beam current measurement without DC bias was done in order to establish the relative phasing between gun and laser. A small current of approximately 20 nA at negative decelerating laser phases provides a measure for dark current. The beam current rises linearly up to 10° laser phase then the whole electron bunch is accelerated in the gun cavity. Due to Schottky effect, the electron beam current is further increased. Finally, the gun cavity design (3.5 cells) limits the plateau length.

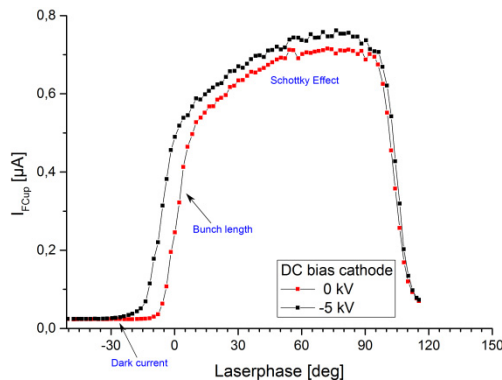


Figure 2: Schottky Scan.

The emission time can be extracted from the slope of the graph. Assuming a Gaussian longitudinal bunch distribution the slope of the beam current can be fitted with a Gauss error function (Eqn. 1) as shown in Fig. 3.

$$F(x) = \frac{1}{2} \left(1 + \operatorname{erf} \left(\frac{x - \mu}{\sqrt{2}\sigma} \right) \right) \quad (1)$$

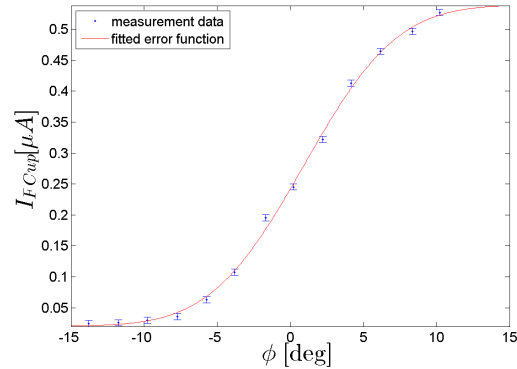


Figure 3: Bunch length estimation from error function fit.

An emission length σ_t of $10.7 \pm 2.6 \text{ ps}$ is calculated from the fit parameter. Compared to the 6 ps laser pulse the evaluated bunch length is overestimated by at least 4 ps due to the fit quality as well as the accuracy of the displayed laser phase ($\pm 0.5^\circ$). Furthermore, the rising Schottky effect as well as beam dynamics will influence the measurement values at the end of the slope. Nevertheless, the Schottky scan can be used to estimate the bunch emission length and provides an important control tool in the commissioning procedure.

LONGITUDINAL PHASE SPACE

Phase Scan Technique

The beam characterization of the longitudinal phase space is performed using the phase scan technique illustrated in Fig. 4. Accelerated in a RF cavity module each bunch of finite length receives an energy chirp in longitudinal direction. After passing a dispersive beampath element e.g. a dipole, the energy spectrum is projected in the transverse plane. In the phase scan technique the longitudinal phase space distribution is measured for different RF phases of the linac cavity. Analysis provides the longitudinal parameters at the cavity entrance.

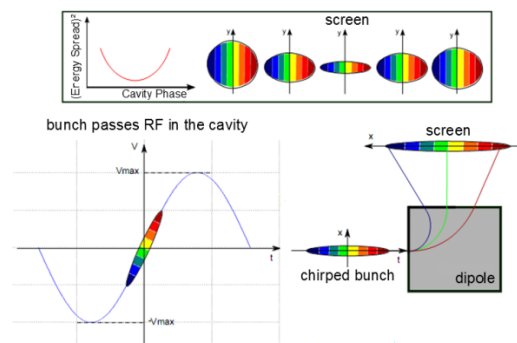


Figure 4: Illustration of phase scan technique [4].

The assumed longitudinal beam ellipse can be defined by

$$\tau = \begin{pmatrix} \tau_{11} & \tau_{12} \\ \tau_{12} & \tau_{22} \end{pmatrix} = \begin{pmatrix} \sigma_z^2 & \tau_{12} \\ \tau_{12} & \sigma_E^2 \end{pmatrix} \quad (2)$$

In this matrix the element τ_{11} describes the rms bunch length squared σ_z^2 and the element τ_{22} is the rms energy spread squared σ_E^2 [5]. During the phase space measurement the RF phase of the second cavity module in Linac 1 is varied. The first dipole of the chicane acts as a spectrometer. The transverse distribution behind the dipole and therefore the energy spread can be resolved on a YAG screen. The distribution is recorded using a CCD camera.

The transformation matrix of the longitudinal beam ellipse is determined by the linac cavity as well as the drift space up to the imaging point of the dipole onto the screen. Since the electron beam reaches relativistic velocity behind the linac module the drift space transfer matrix in the longitudinal phase space can be written as a unit matrix. Therefore, only the transformation of the beam matrix through the linac (Eqn. (3)) must be considered assuming a simple energy boost from the linac:

$$R_{Linac} = \begin{pmatrix} 1 & 0 \\ -2\pi\lambda_{HF} \frac{\Delta E}{E_0} \sin\phi_0 & 1 \end{pmatrix} \quad (3)$$

ϕ_0 describes the RF phase of the reference electron. λ_{HF} is the RF wavelength while $\Delta E/E_0$ specifies the relative energy gain in linac C2. The longitudinal beam ellipse $\tau(1)$ at exit of cavity C2 is given by

$$\tau(1) = R_{Linac} \cdot \tau(0) \cdot R_{Linac}^T \quad (4)$$

Multiplying the matrices of Eqn. (4) matrix element $\tau_{22}(1)$ gives energy spread squared behind the linac, respectively on the YAG screen:

$$\delta_1^2 = \frac{4\pi^2\sigma_z^2}{\lambda_{HF}^2} \left(\frac{\Delta E}{E_0}\right)^2 (\sin\phi_0)^2 - 2\frac{2\pi\tau_{12}\Delta E}{\lambda_{HF}E_0} \sin\phi_0 + \delta_0^2 \quad (5)$$

The measured rms energy spread on the YAG screen for several linac phases ϕ_0 are fit with this parabola function in order to obtain the three matrix elements for the longitudinal phase space in front of linac module C2.

The rms bunch length determines the parabola width, while the correlated energy spread is obtained at $\phi_0=0$. An offset in the vertex occurs due to the uncorrelated energy spread. The parabola vertex shift from $\phi_0=0$ indicates correlation with the laser phase in the SRF gun.

Besides the rms bunch length and rms energy spread the longitudinal emittance can be calculated from the fit parameters (Eqn. (6)). The normalized longitudinal emittance is defined as

$$\varepsilon_{long,n} = \beta\gamma \sqrt{\delta_0^2\sigma_z^2 - \tau_{12}^2} \quad (6)$$

Experimental Results and Discussion

The energy spread for a range of linac phases ϕ_0 was observed for four different gun laser phases. Besides a small laser phase of 10.1° three measurements around the gun minimum energy spread at approximately 57° were performed. Figure 5 presents all experimental results together with their fits.

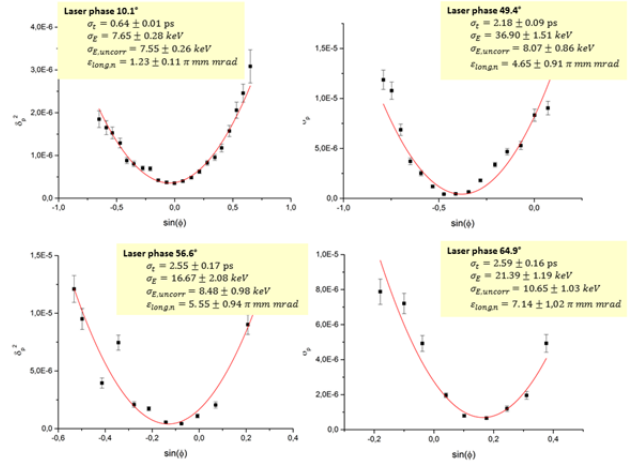


Figure 5: Energy spread measurement for four different laser phases with 19 MeV electron beam.

The measured correlated energy spreads represent the two energy spread minima from the SRF gun at low laser phase as well as at approximately 57° . The vertex shift at both minima is zero. Since there is no significant space charge effect due to the low bunch charge, thermal and RF contributions dominate the uncorrelated energy spread which is nearly constant at 8 keV. Our measurement results confirm the vertex shift correlation with the gun laser phase.

The bunch length is shorter than the rms laser pulse length of 6 ps, slightly reduced by RF bunch compression due to the energy chirp imparted to the beam in the RF field of the gun. Furthermore, bunch lengths seem to grow linearly with laser phase and therefore with bunch charge as evaluated in the Schottky scan in the range $[10^\circ, 90^\circ]$. The longitudinal emittance shows this linear dependence, as well [see Fig. 6][6].

All error bars shown in Fig. 5 take into account the 12 bit read out resolution of the CCD camera. The deviation of each illuminated pixel is estimated to one bin. Simulations confirm that the pixel resolution can be neglected than more than eleven pixels in diameter are illuminated. The parabola fits in the energy spread distribution measurements are weighted to the error bars. All specified errors for the calculated parameters of the longitudinal phase space refer to the standard deviation of the fit parameters weighted by the resolution of the CCD camera.

In order to investigate space charge effects further beam dynamic measurements are planned. The copper cathode will be replaced by Mg and Cs₂Te photocathodes which provide higher quantum efficiencies in order to obtain higher bunch charges. Further dark current and beam halo measurements will be attempted using the proposed wire scanner.

REFERENCES

- [1] J. Teichert et al., “Commissioning of an Improved Superconducting RF Photoinjector at ELBE”, THP061, Proceedings of FEL’14, Basel, Switzerland (2014).
- [2] J. Teichert et al., “Evaluation of Critical R&D Issues of SRF Guns”, EuCARD SRF Review 2011.
- [3] T. Kamps et al., Rev. Sci. Instrum., 79 (2008) p. 093301.
- [4] J. Rudolph, ”Bunch Length Measurements and Status of the Slice Diagnostics System for ELBE/SCRF Gun”, EuCARD SRF Review 2010.
- [5] D.H.. Dowell et al., Nucl. Instr. and Meth. A 507 (2003) 331.
- [6] S. Kashiwagi et al., “Photo-electron beam longitudinal phase space tomography studies at the ATF”, Proceedings of LINAC’00, Monterey, California (2000).